# Identity of the Exchangeable Sulfur-Containing Ligand at the Mo(V) Center of R160Q Human Sulfite Oxidase

Eric L. Klein,[†] Arnold M. Raitsimring,[†] Andrei V. Astashkin,[†] Asha Rajapakshe,[†] Kayunta Johnson-Winters,[†] Anna R. Arnold,[†] Alexey Potapov,[§] Daniella Goldfarb,[§] and John H. Enemark*,[†]

[†]Department of Chemistry and Biochemistry, 1306 East University Boulevard, University of Arizona, Tucson, Arizona 85721-0041, United States

[§]Department of Chemical Physics, Weizmann Institute of Science, Rehovot 76100, Israel

S *Supporting Information*
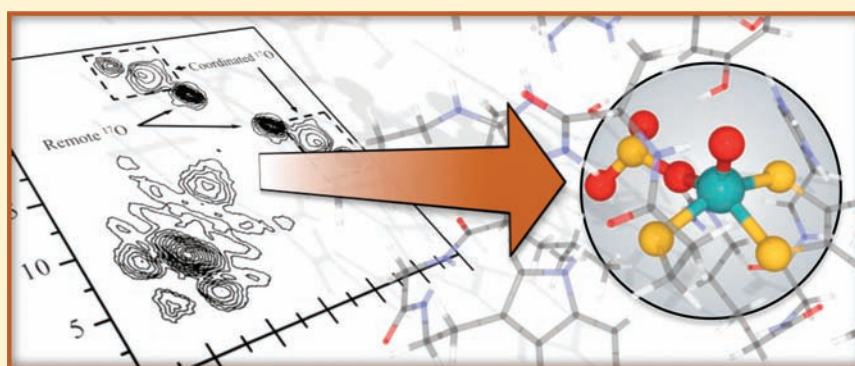
ABSTRACT: In our previous study of the fatal R160Q mutant of human sulfite oxidase (hSO) at low pH (Astashkin et al. *J. Am. Chem. Soc.* **2008**, *130*, 8471−8480), a new Mo(V) species, denoted "species 1", was observed at low pH values. Species 1 was ascribed to a six-coordinate Mo(V) center with an exchangeable terminal oxo ligand and an equatorial sulfate group on the basis of pulsed EPR spectroscopy and ^{33}S and ^{17}O labeling. Here we report new results for species 1 of R160Q based on substitution of the sulfur-containing ligand by a phosphate group, pulsed EPR spectroscopy in K_a- and W-bands, and extensive density functional theory (DFT) calculations applied to large, more realistic molecular models of the enzyme active site. The combined results unambiguously show that species 1 has an equatorial sulfite as the *only* exchangeable ligand. The two types of ^{17}O signals that are observed arise from the coordinated and remote oxygen atoms of the sulfite ligand. A typical five-coordinate Mo(V) site is compatible with the observed and calculated EPR parameters.

INTRODUCTION

Sulfite oxidizing enzymes (SOEs), including prokaryotic sulfite dehydrogenase (SDH) and eukaryotic sulfite oxidase (SO), are biologically ubiquitous and catalyze the two-electron oxidation of sulfite (SO_3^{2-}) to sulfate (SO_4^{2-}).[1,2] SO is vital for normal neonatal neurological development in humans.[3−5] All known SOEs possess a five-coordinate molybdenum active center that has an approximately square-pyramidal geometry, with an axial oxo ligand, three nonexchangeable equatorial sulfur ligands, and an exchangeable equatorial ligand (Figure 1).[6−10] Two of the sulfur ligands are provided by the pyranopterindithiolate cofactor (also called "molybdopterin", MPT), and one sulfur ligand comes from a conserved cysteine residue.

The identity of the exchangeable equatorial ligand, which occupies the substrate binding pocket, depends on the stage of the catalytic cycle, during which the molybdenum is reduced from Mo(VI) to Mo(IV) upon binding sulfite and is then reoxidized by two successive intramolecular electron transfer steps through a Mo(V) intermediate.[11] In SDH and all

nonplant forms of SO, integral heme centers accept the electrons from the reduced molybdenum center.

The intermediate Mo(V) state is paramagnetic ($S = 1/2$), and electron paramagnetic resonance (EPR) spectroscopy has been instrumental in providing information about the nature and geometry of the exchangeable ligand and its role in the catalytic cycle as a function of pH, organism, mutation, and the presence of specific anions in the buffer.[11−18] The results of numerous EPR investigations, which involved high-resolution pulsed EPR techniques such as electron spin echo, envelope modulation (ESEEM), and pulsed electron−nuclear double resonance (ENDOR), have been summarized in recent reviews.[11,19] For wild type (*wt*) vertebrate SO in the Mo(V) state and in the absence of inhibiting anions (*e.g.*, PO_4^{3-}, AsO_4^{3-}), the exchangeable equatorial ligand is known to be hydroxide.[20] The orientation of this ^-OH ligand depends on the buffer pH,
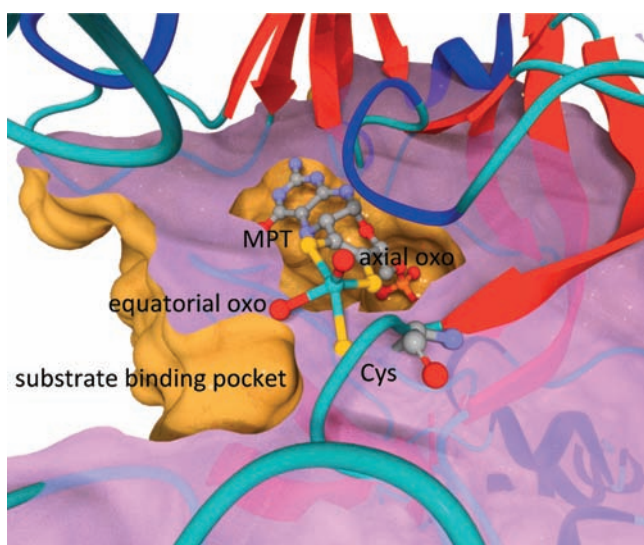
Figure 1. Active site of SO rendered from the 1.9 Å chicken SO structure, pdb 1SOX.[6] The molybdopterin (MPT), the conserved Mo-bound Cys residue (C185 and C207 in chicken and human SO, respectively), the axial and equatorial oxo ligands, and Mo are shown as a ball-and-stick model (blue-green = Mo, red = O, yellow = S, gray = C, orange = P, and purple = N). The protein is displayed as ribbons and a cross section to reveal the surfaces of the substrate and cofactor pockets and their relative orientations.

Scheme 1. Preparations of the Various R160Q hSO Species and Schematic Representations of Each of Their 5-Coordinate Mo Centers[a]

[a]The straight lines in the chemical structures denote the coordinated sulfur atoms from the conserved cysteine and the MPT (Figure 1).

however, and the corresponding structural forms, which result in very different EPR spectra, were historically labeled "low-pH" (*lpH*, pH ≤ 7) and "high-pH" (*hpH*, pH ≥ 9).[13,21]

Quite different spectroscopic results were obtained for the low-pH sample of plant SO from *Arabidopsis thaliana* (At-SO), however, where the two-electron reduction of the Mo(VI) center with sulfite was followed by a one-electron oxidation by ferricyanide[22] and resulted in the Mo(V) being coordinated by a substrate-derived ligand that was assigned as sulfate,[23,24] in agreement with the proposed product-bound intermediate in the catalytic cycle.[1] This form of SO was called *blocked*, based on a hypothesis that the sulfate product was shielded from hydrolysis by some steric block, creating a trapped enzyme−product (EP) complex. A similar type of *blocked* form was also obtained for low-pH samples of various SOE mutants[25,26] and for the chloride-depleted low-pH samples of *wt* human SO (hSO).[27]

Most SO samples prepared in the absence of inhibiting anions give EPR spectra that correspond to the normal *hpH*, *lpH*, and *blocked* forms described above. The R160Q human SO (hSO) mutant, however, produces very different EPR spectra at low and intermediate pH values (pH ≤ 8).[28] In this clinically important mutant, the arginine residue (R160) located next to the Mo ion, *trans* to the apical oxo ligand, is replaced by glutamine. The structural modifications effected by this mutation dramatically alter the EPR spectra observed at low and intermediate pH values. Instead of the regular *lpH* species, having an exchangeable −OH ligand, being observed, a variation of the *blocked* form (denoted "species 1") is detected at low pH. At intermediate pH values, another variant (denoted "species 2") is observed, with a maximum yield obtained at about pH 7. At high pH, the usual *hpH* species is formed. The conditions for formation of species 1 and 2 and other species that are related to this work are presented in Scheme 1.

Species 1 has been characterized in some detail by pulsed EPR methods using both [33]S-enriched sulfite and [17]O-enriched
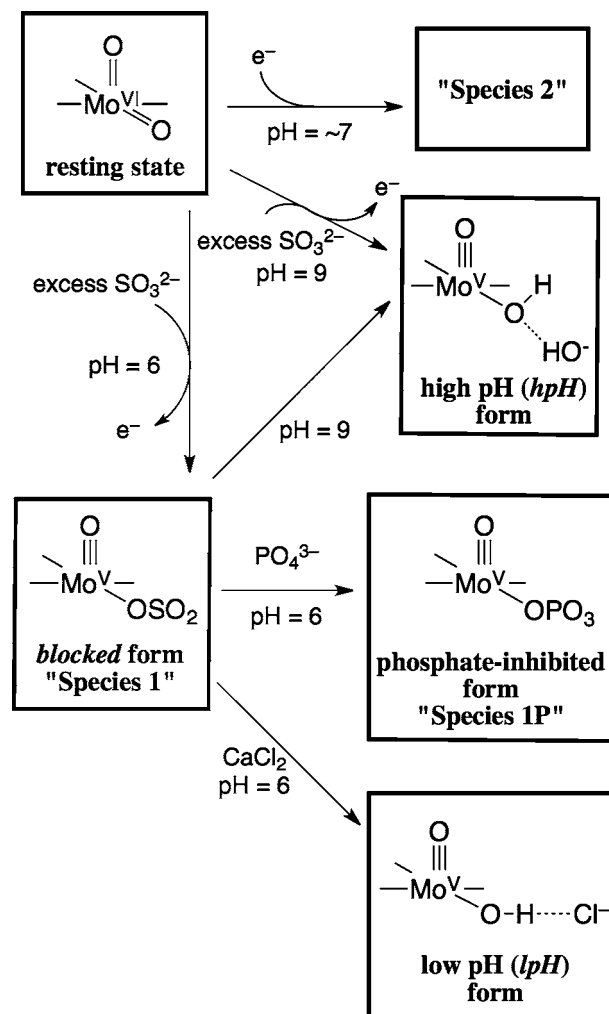
water.[11,27] The observation of characteristic [33]S ESEEM has established that species 1 is indeed a *blocked* form, as was initially postulated on the basis of the lack of an observable −OH ligand proton.[24] [17]O ESEEM has revealed two types of oxygen nuclei: (1) a strongly coupled oxygen with a hyperfine interaction (*hfi*) constant (*A*) of ~18 MHz and (2) a weakly coupled oxygen with $A \cong 5$ MHz. The strongly and weakly coupled oxygen signals were initially assigned to the exchangeable equatorial ligand and to the oxo ligand, respectively.[11] Compared to the oxo ligand of the model oxo-molybdenum compound $[Mo(V)^{17}O(SPh)_4]^{-}$,[29] or of *hpH* SO,[30] the assigned oxo ligand of species 1 was found to have a significantly larger nuclear quadrupole interaction (*nqi*) with a nuclear quadrupole coupling constant ($\chi \equiv e^2Qq/h$) of ~5 MHz. The substantially larger value of χ for R160Q hSO (4× that of either $[Mo(V)^{17}O(SPh)_4]^{-}$ or *hpH* SO) was tentatively explained by the possibility of Q160 coordinating to Mo(V) *trans* to the axial oxo group to form a 6-coordinate metal center with a weakened oxo-Mo(V) bond.[31] A six-coordinate Mo center involving glutamine coordination was proposed previously for R160Q by Doonan et al.[28] Results from a

6-coordinate oxo-Mo(V) model compound, (dttd)Mo(V)^{17}O-(^{17}OTMS), further supported this idea.[31] Our subsequent research, however, based largely on density functional theory (DFT) results,[11] including new results reported in this work, has led us to reject this hypothesis as well as the entire premise that the equatorial ligand of the *blocked* species should, in fact, be assigned to a sulfate ligand.

A more fundamental consideration of the experimental results to date also creates additional doubt regarding the assignment of sulfate as the equatorial ligand of the *blocked* forms. The relatively large values of χ measured for the ^{33}S of several *blocked* forms (ranging from 26 to 40 MHz),[23,25,27,31] for example, appear to be far too large to originate from a sulfur nucleus located at the center of the very symmetric electric field created within sulfate (which is tetrahedral and should give a χ value for ^{33}S that approaches zero).[11] The less symmetric electric field gradient created by trigonal pyramidal sulfite, however, should produce a strong ^{33}S *nqi*. Indeed, our recent preliminary DFT calculations support this notion.[11] Also, since the *blocked* forms, including species 1, are all observed at low pH, exchange of the oxo ligand is unlikely, since the yield of the ^{17}O-labeled oxo ligand in *lpH* SO is negligible, even after incubation of the sample in ^{17}O-enriched buffer over many hours.[31] In contrast, a measurable yield of ^{17}O-labeled oxo was observed in *hpH* SO for similar incubation times.[32] Although the exact mechanism(s) of the oxo ligand exchange is not clear, these experiments indicate that the exchange should involve a hydroxide, which would be favored at higher buffer pH values. An additional consideration in analysis of the ^{17}O-labeling results is that all of the oxygen atoms of sulfite exchange rapidly in water.[33] Therefore, the observed weakly coupled ^{17}O could potentially be assigned to one of the remote oxygen atoms of the equatorial ligand instead of to the oxo. This alternative explanation could account for the larger ^{17}O χ for the "oxo" of *blocked* R160Q hSO.

As part of our effort in this work to determine the identity of the equatorial ligand of species 1, here we report the simultaneous disappearance of the weakly coupled ^{17}O ESEEM and emergence of ^{31}P ESEEM (from the generated phosphate form)[14] upon addition of phosphate to the buffer. This result indicates that the weakly coupled oxygen must belong to the exchangeable equatorial ligand and not to the axial oxo, in contrast to previous assignments.[31] Additional pulsed EPR measurements for the strongly coupled equatorial ^{17}O, in conjunction with extensive DFT calculations, have allowed the ^{17}O and ^{33}S spectroscopic parameters of all of these atoms to be approximated, thereby clarifying the identity of the equatorial ligand in species 1. The new results presented here show that the *blocked* form of SOEs results from the coordination of substrate (sulfite), which is present in excess in *in vitro* studies, rather than from the coordination of product (sulfate) to the Mo(V) center.

■ MATERIALS AND METHODS

Sample Preparation. Recombinant R160Q hSO was expressed and purified as previously described.[31] The samples of R160Q hSO at low pH in ^{17}O-enriched water were prepared by first concentrating a 200 μL solution of the enzyme in 25 mM Bicine and 25 mM Pipes at pH 6.2 to reduce the amount of natural abundance water. Next, a solution of 25 mM Bicine and 25 mM Pipes buffer was vacuum centrifuged to evaporate the natural abundance water, and the pelleted buffer was redissolved in the same volume of H$_2$^{17}O. The concentrated enzyme sample was then incubated for approximately 3 h at 4 °C in 30 μL of the buffer prepared with H$_2$^{17}O. Finally, the enzyme was

reduced with a 20-fold excess sodium sulfite under argon, and the samples were immediately frozen in liquid nitrogen. The initial concentration of enzyme in the Mo(V) state was about 0.5 mM. For the ligand exchange experiments, a large excess of phosphate buffer or CaCl$_2$ was added, and the thawed samples were then refrozen. The specific relative amounts of these reagents are given in the corresponding figure captions for each experiment. ^{17}O-enriched, pH 5.4 phosphate buffer was prepared by vacuum centrifuging a 100 μL solution of 500 mM phosphate buffer prepared with natural abundance water, followed by redissolving the resulting buffer pellet into the same volume of ^{17}O-enriched water. For all of these experiments, >90 atom % ^{17}O-enriched water (Aldrich 609862) was used.

Pulsed EPR Experiments. Pulsed EPR experiments were performed in two microwave (mw) bands. K$_a$-band (∼30 GHz) measurements were performed on the home-built broadband spectrometer at the University of Arizona EPR Facility.[34] W-band (∼95 GHz) experiments were performed on the home-built pulsed spectrometer at the Weizmann Institute of Science (Israel).[35] Data processing, which included standard low-order spline procedures for baseline removal, apodization, Fourier transforms, linear phase corrections to account for dead-time effects, and symmetrization of 2D (two-dimensional) HYSCORE (HYperfine Sublevel CORrelation spectroscopy)[36] in some cases, was performed using the SpecLab software,[37] which is available free-of-charge online and includes detailed instructions for all of these procedures. Specific details of the experimental conditions are provided in the figure captions where appropriate.

DFT Calculations. The ORCA computational package (version 2.8.0) was used for all quantum-chemical calculations.[38] BP86[39,40] and B3LYP[41,42] functionals were used for the geometry optimization and property calculations, respectively, in conjunction with Ahlrich's all-electron TZVP basis set.[43−45] Relativistic effects were treated at the level of the zeroth order regular approximation (ZORA)[46] in one-component form using the model potential of van Wüllen[47] (as implemented in ORCA). For geometry optimizations, the one-center ZORA relativistic correction was used.[48] The protein environment was modeled through dielectric continuum methods (conductor-like screening model, COSMO)[49] using a dielectric constant of four.[50]

Starting coordinates for the sulfate-bound model were prepared by modifying the solvent-exposed (equatorial) oxo ligand of the cSO crystal structure (pbd 1SOX)[6] to a sulfato group and by selecting nearby amino acid residues (or fragments) and water molecules that define the substrate binding pocket and other important H-bonding interactions. This was done so that the geometry optimization step could be performed with as few biased geometric constraints as possible and so that the electric field gradient around the ligands could be modeled as accurately as possible, thus improving the general quality and significance of the final results. The geometry optimization calculation was carried out with only the protein backbone α carbon atoms (or the residue side chain carbon closest to the α position where the backbone was not required) and water oxygen atoms constrained to their relative Cartesian coordinates, leaving all other atoms fully relaxed. The starting coordinates for the models with bound sulfite were prepared from the optimized sulfate model by successively removing the remote oxygen atoms from sulfate and then optimizing the models and calculating their properties as described for the sulfate model. The optimized atom coordinates for the sulfate- and sulfite-bound models, from which all properties were calculated, are provided in the Supporting Information.

■ RESULTS AND DISCUSSION

Sulfur-Containing Ligand Displacement Experiments. Several experiments were performed to displace the sulfur-containing exchangeable ligand of species 1 by adding either phosphate or CaCl$_2$. The incentive for the phosphate experiments was outlined in the Introduction. The experiments involving the addition of CaCl$_2$, however, were based on the presumption that it should be possible to shift the equilibrium

1410

dx.doi.org/10.1021/ic201643t | *Inorg. Chem.* 2012, 51, 1408−1418

from species 1 toward species 2 if the exchangeable ligand were sulfite. More specifically, the addition of $CaCl_2$ to species 1 should produce $CaSO_3$, which is only slightly soluble in water.[51,52] Chloride occupies the binding pocket of the *wt lpH* forms of SO, as we have previously demonstrated,[18,27] but it does not appear to be involved in the formation of the *lpH* forms of R160Q.[53] In the case of sulfate coordination, however, no effect of $CaCl_2$ on the equilibrium would be expected, since the solubility of $CaSO_4$ in water is relatively high.[54] The limited amount of available purified enzyme restricted the number of conditions that could be tested to determine the effects of pH or the concentration of either phosphate or $CaCl_2$ on the experimental results. The full results of the $CaCl_2$ experiments, as well as the results of the phosphate experiments that are not presented in the main text, are provided in the Supporting Information. The $CaCl_2$ experiments unexpectedly showed the conversion of species 1 into the standard *lpH* form, *not* into species 2. The detailed results of one of the phosphate experiments are described in the following section.

The solid trace in Figure 2a shows the K_a-band field sweep echo-detected spectrum of R160Q hSO at pH 6.4. Species 1
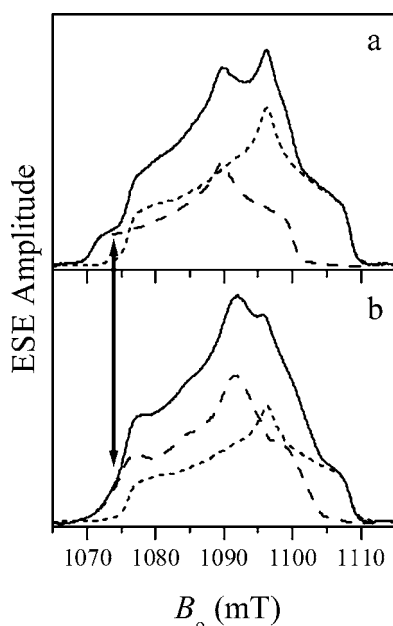

Figure 2. K_a-band ESE-detected field sweep spectra of R160Q hSO (primary ESE). (a) Solid trace, the spectrum of the original sample at pH = 6.4, which contains contributions from species 1 (long-dashed trace) and species 2 (short-dashed trace). (b) Solid trace, the spectrum obtained after adding phosphate buffer, where the final concentration of phosphate was ~200 mM. The short- and long-dashed traces show the contributions from species 2 and 1P (formed from species 1). The spectrum of species 1P (long-dashed) is the difference between the solid and short-dashed traces. Experimental conditions: mw frequency = 30.068 GHz; mw pulses, 2 × 12 ns; time interval between the mw pulses, τ = 200 ns; temperature = 21 K. The arrow shows the EPR position at which the ESEEM spectra of Figures 3 and 4 were obtained (B_o = 1074 mT).

and species 2 both contribute to this spectrum. The individual spectra of species 1 and 2, obtained under different experimental conditions, are shown in the same figure by long- and short-dashed traces, respectively. The ESE field sweep spectrum obtained subsequent to the addition of phosphate buffer is shown by the solid trace in Figure 2b. As

in Figure 2a, the short-dashed trace shows the contribution of species 2. The disappearance of the characteristic low-field shoulder at $B_o \cong 1070-1075$ mT, as well as changes in the central part of the spectrum, indicate that species 1 was transformed into a different type of Mo(V) center, presumably a phosphate-coordinated species (species 1P). This is shown by the difference between the experimental solid trace and the appropriately normalized spectrum of species 2 as the long-dashed trace in Figure 2b. The principal g-values of species 1P, $(g_x, g_y, g_z) \approx (1.950, 1.968, 1.999)$, are somewhat different from those observed for the phosphate-inhibited (P_i) species of *wt* vertebrate SO, $(g_x, g_y, g_z) \approx (1.961, 1.969, 1.992)$.[14] Since there is significant disagreement between the g-values of species 1P and P_i, the g-values do not confirm the generation of P_i. For this reason, ESEEM experiments were performed to establish the presence of the phosphate ligand in this newly generated form.

Figure 3 shows the cosine Fourier transformation (FT) spectra of the two-pulse ESEEM traces recorded at the EPR
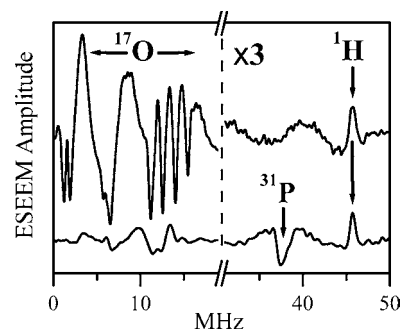
Figure 3. K_a-band two-pulse ESEEM spectra (cosine FT) of species 1 (upper trace) and species 1P (lower trace) obtained at the EPR position indicated by the arrow in Figure 2. Experimental conditions: mw frequency = 30.068 GHz; B_o = 1074 mT; mw pulses, 2 × 12 ns; temperature = 21 K. For clarity, the modulation amplitudes to the right of the break in the x-axis have been magnified by a factor of 3. The proton matrix line is marked by the arrow labeled "^{1}H" (at ~46 MHz, which corresponds to the ^{1}H Larmor frequency, ν_H). Likewise, the arrow labeled "^{31}P" indicates the position of the sum combination line of ^{31}P (ν_σ = ~37.5 MHz), which is close to double the Larmor frequency of ^{31}P at this magnetic field, $2\nu_P \approx 37.1$ MHz.

position indicated by the arrow in Figure 2. At this position the relative contribution of species 1P is maximized. The upper trace in Figure 3 corresponds to the initial sample and is primarily contributed to by species 1. The lower trace corresponds to the sample after the addition of phosphate buffer and is contributed to primarily by species 1P. Two features of the species 1P ESEEM spectrum are most interesting within the context of this investigation. The first feature is the sum combination line of ^{31}P ($\nu_\sigma \sim 37.5$ MHz), which indicates the presence of a nearby ^{31}P nucleus. The second is the dramatic decrease of the ^{17}O ESEEM compared to the spectrum prior to the introduction of phosphate buffer. It is significant that only the sum combination line of the nearby ^{31}P nucleus is observed in this ESEEM spectrum, while the fundamental lines are not readily observable. This situation mirrors that of the usual P_i species of *wt* SO[12] and can be explained by the large width of the fundamental lines, which diminishes their amplitudes.

To observe the fundamental lines of ^{31}P and to estimate the *hfi*, hyperfine sublevel correlation (HYSCORE)[36] spectroscopy was used. Figure 4 shows the HYSCORE spectrum obtained at
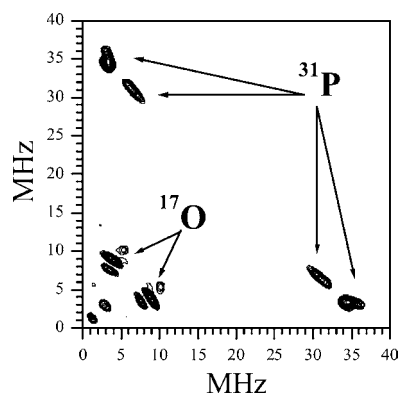
Figure 4. K_a-band HYSCORE spectrum of species 1P obtained at the EPR position indicated by the arrow in Figure 2. Experimental conditions: mw frequency = 30.068 GHz; B_o = 1074 mT; mw pulses, 12, 12, 22, and 12 ns; temperature = 21 K. The spectrum represents the sum of the spectra recorded at the time intervals (τ) between the first two mw pulses for 150, 180, and 210 ns. The arrows labeled "^{31}P" point at the ^{31}P fundamental lines, and the arrows labeled "^{17}O" indicate the lines of ^{17}O from H-bonded water.

the EPR position indicated by the arrow in Figure 2. The cross peaks in the ranges 29−37 MHz and 8−2 MHz are centered at the ^{31}P Zeeman frequency, $\nu_P \approx 18.5$ MHz, and are thus assigned to ^{31}P. The line shapes of the ^{31}P cross peaks indicate that the ^{31}P species most probably exists in several structural conformations, as was suggested by Dikanov et al. in similar studies.[55] Measurements across the entire range of the species 1P EPR spectrum (see Supporting Information Figure S3) reveal that the ^{31}P hfi varies within the range of about 21−43 MHz. A hfi constant of this magnitude is typical of phosphate that is coordinated to Mo(V).[12] On the basis of this strong correlation, we conclude that species 1P is indeed a phosphate-coordinated form of R160Q_hSO.

The dramatic decrease of the ^{17}O ESEEM in species 1P (Figure 3) indicates that the weakly coupled oxygen responsible for the intense sum combination features of species 1 (Figure 3, upper trace) does not originate from the oxo ligand but rather from one of the remote oxygens of the sulfur-containing ligand. In species 1P, this ligand is displaced by naturally abundant phosphate (^{31}P^{16}O$_4^{3-}$), and the initial ^{17}O ESEEM features disappear. Nevertheless, the HYSCORE spectrum of Figure 4 clearly shows signals centered at the ^{17}O Zeeman frequency, $\nu_O \approx 6.2$ MHz, that have resolved quadrupole splittings. The intensities of these contours are similar to those of ^{31}P. These may also originate from a residual amount of species 1, from species 2, and/or from nearby water that is coordinated to the phosphate. The sulfur-containing ligand, whether sulfite or sulfate, possesses either two or three remote (noncoordinated) oxygens. Only one of these remote ^{17}O nuclei is observed experimentally; however, since the hfi parameters of these oxygens strongly depend on the orientation of the ligand with respect to the Mo(V) d_{xy} orbital.[30] This, as well as the specific identity of the equatorial ligand in species 1 (sulfate or sulfite), will be addressed in detail using DFT calculations (vide infra).

Pulsed EPR Measurements for the Coordinated ^{17}O of the Sulfur-Containing Ligand. With regard to the Mo(V)-coordinated oxygen of the sulfur-containing ligand, earlier K_a-band HYSCORE measurements have only been able to evaluate the hfi constant at the g_y EPR position ($A \sim 18$ MHz),[31] since the ESEEM of this nucleus could not be detected at any other EPR position. Furthermore, no information about the nqi of this ^{17}O

was obtained, since the nqi splittings were not resolved. Zeeman and hyperfine interactions that are close to mutual cancellation in K_a-band can produce pronounced detrimental effects on the nondiagonal elements of the anisotropic hfi and nqi. This may explain the complications involved in observing the nqi. To determine the nqi of the strongly coupled ^{17}O as well as the anisotropy of its hfi, we performed W-band (~95 GHz) ESEEM and ELDOR (electron−electron double resonance) detected NMR (ED-NMR) measurements on R160Q_hSO. In W-band, the coordinated equatorial ^{17}O is expected to be well within the weak hfi regime, $\nu_O > A/2$ (where $\nu_O \sim 20$ MHz is the Larmor frequency of ^{17}O), which should decrease the broadening that results from nondiagonal elements of the hfi and nqi. In addition, better orientation selection may lead to narrower and better-resolved signals.

ED-NMR is a useful method for measuring fundamental frequencies. It was first proposed and demonstrated at X-band frequencies.[56] Because of the relatively low nuclear Larmor frequencies at ~0.35 T, however, this method has not been very popular in instances of small hyperfine couplings. At higher fields (such as those encountered at K_a- and W-bands), however, the technique is more practical due to the increased nuclear Larmor frequencies, especially for low γ nuclei.[57−61] The S/N ratio for the fundamental line is often sufficiently better than that of either ENDOR or HYSCORE, such that a series of spectra at different positions along the EPR powder pattern can be acquired in a relatively short time. The disadvantage of this technique is its lower resolution as compared to either ESEEM or ENDOR.

The ED-NMR and W-band echo-detected EPR spectra of species 1 are shown in Figure 5. The largest hyperfine coupling
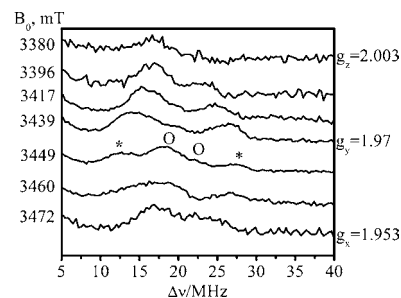

Figure 5. ED-NMR spectra of species 1 measured at different magnetic field positions (indicated on the left side of each trace). The largest hyperfine coupling (observed at 3449 mT) is labeled by "∗". The spectral features of the weakly coupled ^{17}O (observable on the same trace and labeled by "O") are centered about the ^{17}O Larmor frequency ($\nu_O \sim 20$ MHz) and are separated by ~4.5 MHz. The field positions of g_x, g_y, and g_z that correspond to the labeled traces are shown in Figure S6. Experimental conditions: preparation (probing) mw pulse = 10 μs; the observation two-pulse sequence consisted of 100 ns ($\pi/2$) and 200 ns (π) pulses separated by a time interval (τ) of 400 ns. The time interval between the preparation and observation pulses was 10 μs; observation mw frequency = 94.897 GHz; temperature = 21 K.

(marked with "∗") of ~16 MHz is observed at a field of 3449 mT, which is slightly off g_y. Another doublet of ~4.5 MHz, and centered about the ^{17}O Larmor frequency ($\nu_O \sim 20$ MHz), is observed as well (marked with "O"). At g_z and g_x, the splittings are ~7 MHz and 8−9 MHz, respectively. The largest splitting observed in the W-band is somewhat smaller than that of the K_a-band (18 MHz), which might be attributable to larger line

1412

dx.doi.org/10.1021/ic201643t | Inorg. Chem. 2012, 51, 1408−1418

widths in the W-band. Despite the benefits offered by ED-NMR for measuring *hfi*, unfortunately, the *nqi*-related splittings of the ^{17}O nuclei in species 1 could not be resolved. Therefore, ESEEM measurements were carried out to resolve the quadrupole interactions.

W-band ESEEM measurements were performed at each of the EPR turning points. While the measurements at g_x and g_y provided useful data, the ESEEM amplitude at g_z was apparently too small to give meaningful data. Figure 6a
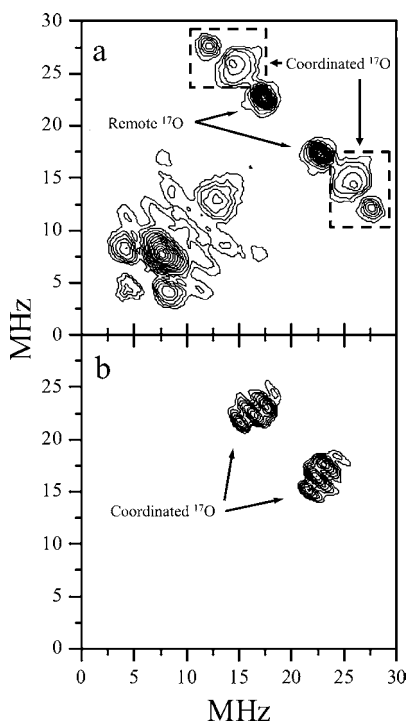
Figure 6. W-band HYSCORE spectra of species 1 obtained at the g_y (a) and g_x (b) EPR spectrum positions. The spectra represent the sums of the spectra that were obtained at time intervals (τ) between the first two mw pulses of 137 and 175 ns. The correlation lines of coordinated and remote ^{17}O are indicated. Experimental conditions: mw frequency = 94.897 GHz; B_o = 3441.7 mT (a) and 3472.9 mT (b); mw pulses = 12.5, 12.5, 25, and 12.5 ns; temperature = 21 K.

shows the W-band HYSCORE spectrum of species 1 obtained at g_y. The correlation peaks located symmetrically with respect to the ^{17}O Larmor frequency are consistent with the signals observed from ED-NMR and can be assigned to the remote and coordinated oxygen nuclei. The specific assignments of the ^{17}O nuclei with the features of Figure 6a are based on comparisons with the K_a-band HYSCORE spectra detected at g_y.[31] The outermost features of the correlation peaks, assigned to the coordinated equatorial ^{17}O, are located at about (28, 12) and (12, 28) MHz. These allow the upper limit of the *hfi* constant be estimated as A_Y ~16 MHz, which is slightly smaller than A_Y ~ 17−18 MHz observed in the K_a-band. This difference is most likely caused by underexcitation[62] of the ^{17}O ESEEM, which occurs when the amplitude of the mw field, B_1, is smaller than the typical nuclear transition frequencies.[63] Furthermore, the τ-dependent blind-spots,[36] where τ is the time interval between the first and second mw pulses, may also be partially responsible for the inability to observe the outermost features of the HYSCORE that correspond to the coordinated ^{17}O. In addition, the quadrupole fine structure for

this ^{17}O is not observed in the HYSCORE spectrum obtained at g_y. The spectrum obtained at g_x, in contrast, displays a well-resolved structure with *nqi* splittings between the antidiagonal ridges, $\Delta\nu_Q$, of about 1.1 MHz. Assuming this to be the absolute maximum quadrupole splitting, one could estimate the quadrupole coupling constant as $\chi \approx {}^{20}/_3\Delta\nu_Q \approx 7.3$ MHz.[64] This value is significantly larger than $\chi \approx 4.5$ MHz, which was determined in earlier K_a-band measurements for the remote ^{17}O.[31] Furthermore, the maximum quadrupole-related splitting for the remote oxygen nuclei is observed at g_z and is collapsed at g_x. The features observed in the HYSCORE shown in Figure 6b, therefore, are best assigned to the coordinated ^{17}O of the sulfur-containing ligand. The *hfi* constant at g_x ranges from about 4 to 11 MHz, as measured between the inner and outer edges of the correlation ridges, which is consistent with the ED-NMR data. Since a single-crystal-like HYSCORE spectrum would be expected at the g_x EPR position, the observed range of the *hfi* constants here most likely reflects the structural variability of the equatorial ligand that results in a statistical distribution of both the isotropic and anisotropic *hfi*. Contributions from the remote oxygens can be excluded due to their collapsed quadrupole splittings at g_x as observed in the Ka-band spectrum (Figure 7).
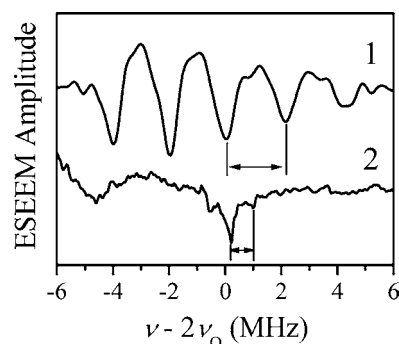
Figure 7. Sum combination line region of the cosine FT spectra of the two-pulse W-band and integrated four-pulse K_a-band ESEEM[68,69] (traces 1 and 2, respectively) obtained at g_x. The quadrupole splittings, $\Delta\nu_Q$, are indicated for each trace. Experimental conditions for trace 1: mw frequency = 94.897 GHz; B_o = 3472.9 mT; mw pulses, 2 × 25 ns; temperature = 21 K. Experimental conditions for trace 2: mw frequency = 29.523 GHz; B_o = 1081 mT; mw pulses, 4 × 15 ns; temperature = 21 K. A frequency of zero is defined as double the ^{17}O Zeeman frequency at the given magnetic fields.

To better estimate the frequency range of the ^{17}O fundamental lines and the range of the *hfi* constants, a blind-spot-free two-pulsed ESEEM technique was used. Figure 8 shows a W-band two-pulse ESEEM spectrum of species 1 obtained at g_y. The major lines, located symmetrically with respect to $\nu_O \approx 19.9$ MHz, are assigned to ^{17}O. The splitting between the maxima of these lines gives a direct reading of the average *hfi* constant at g_y (A = 15 MHz), which clearly demonstrates that these lines belong to the coordinated ^{17}O ligand. The range encompassed between the outermost points of these features defines a *hfi* constant of about 21 MHz. This slightly exceeds the effective *hfi* constant of 18 MHz observed at the K_a-band and may be overestimated since the fundamental lines in two-pulse ESEEM are broadened by the *nqi*. The moderate differences between the *hfi* values measured using ESEEM and ED-NMR are most likely due to the different contributions of the anisotropic *hfi* in
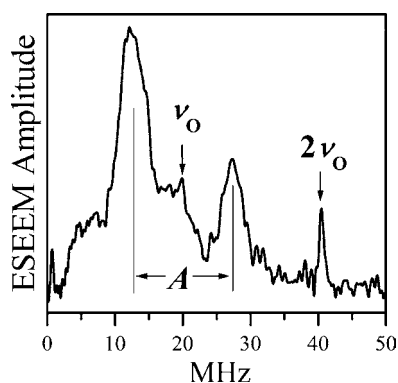
Figure 8. W-band two-pulse ESEEM spectrum of species 1 recorded at g_y. The ^{17}O Larmor (ν_O) and double Larmor ($2\nu_O$) frequencies, and the *hfi* constant (A) of the coordinated ^{17}O are labeled. Experimental conditions: mw pulse durations = 12.5 ns ($\pi/2$) and 25 ns (π); mw frequency = 94.897 GHz; B_o = 3441.7 mT; temperature = 21 K.

the generation of the spectra. Despite this, the spectra obtained using either technique agree qualitatively with each other, and the maximum *hfi* constant of the coordinated ^{17}O estimated from them is about 18 MHz.

Contributions from the remote ^{17}O nuclei are not observable in the g_y ESEEM spectrum in Figure 8 due to their considerably smaller amplitudes. The magnetic resonance parameters of the remote ^{17}O nuclei are closer to the weak *hfi* limit, and their anisotropic *hfi*'s are weaker than those of the coordinated ^{17}O. They do appear in the g_y HYSCORE spectrum, however, as seen in Figure 6, but comparisons of their intensities are problematic due to blind-spot effects and pulse bandwidth limitations.

The most significant result obtained from the W-band primary ESEEM measurements for the coordinated ^{17}O is the observation of the sum combination feature of this nucleus at g_x (Figure 7, trace 1). The average quadrupole splitting, $\Delta\nu_{\sigma Q}$, between the individual features of the sum combination quintet is about 2.1 MHz. The quadrupole coupling constant derived from this splitting, $\chi \approx {}^{10}/_3 \Delta\nu_{\sigma Q} \approx 7$ MHz,[64] is in agreement with the estimate made from the HYSCORE spectrum (Figure 6b). For comparison, Figure 7, trace 2 shows the sum combination

feature of the remote ^{17}O observed at the K_a band. The quadrupole splitting in this spectrum is only about 0.8 MHz, in contrast to that of trace 1. This comparison supports our assignment of the Figure 6b HYSCORE spectrum and the lines of Figure 7, trace 1, to the coordinated ^{17}O of the sulfur-containing equatorial ligand.

A quadrupole coupling constant of about 7 MHz is typical for a ^{17}O with its valence orbitals hybridized to approximately sp³.[64] The fact that the largest quadrupole splitting is observed at g_x indicates that the long axis of the *nqi* tensor is close to the axis of g_x. Notably, this is one of only a few direct measurements of the nuclear quadrupole coupling constant for a ^{17}O nucleus that is directly coordinated to a metal ion. For this reason, this result is also potentially important as a benchmark in other investigations.

The overall range of the *hfi* splittings for the coordinated ^{17}O (about 4 to 20 MHz) gives an idea of its anisotropic *hfi*. Assuming axial *hfi*, the long component of the anisotropic *hfi* tensor can be estimated as $T_\parallel \approx \pm 10$ MHz. This anisotropic *hfi* constant is significantly larger than $T_\parallel \approx -2.5$ MHz, estimated for the dipolar interaction with the unpaired electron situated on Mo(V), and this is explained by the spin delocalization into the oxygen orbitals. For the isotropic *hfi* constant, two estimates are possible, $a_{iso} \approx \pm 9$ MHz or ± 15 MHz, with the first estimate requiring $T_\parallel$ of the same sign as a_{iso} and the second requiring $T_\parallel$ of the opposite sign. From our previous DFT calculations for a hydroxo ligand,[30] we can expect the spin population on the oxygen orbitals to be positive, resulting in negative a_{iso} and $T_\parallel$. Thus, the *hfi* parameters for the coordinated ^{17}O can be estimated as $(a_{iso}, T_\parallel) \approx (-9, -10)$ MHz. These and other relevant spectroscopic parameters, including the parameters obtained from extensive quantum-chemical calculations (*vide infra*), are summarized in Table 1.

In summary, the *blocked* form of R160Q of hSO has at least two types of ^{17}O nuclei (remote and coordinated) that contribute to the various spectra (two-pulse ESEEM, HYSCORE, ED-NMR) at the K_a- and W-bands. Fortunately, the differing dependence of the intensities of the two types of ^{17}O lines on the spectrometer frequency enables them to be resolved. In K_a-band, the remote oxygen was observed throughout the entire EPR spectrum, whereas the coordinated oxygen was only observed at g_y and with no *nqi* resolution. In contrast, at W-band the signals of the remote ^{17}O were weaker, though observed throughout

Table 1. Experimental Magnetic Resonance Parameters for *wt* and Mutant *Blocked* Forms of SO and DFT-Calculated Magnetic Resonance Parameters for the Sulfate- and Sulfite-Bound SO Models

Species		a_{iso}/MHz	(T_{11}, T_{22}, T_{33})/MHz	e^2Qq/h/MHz	η	ref
		hfi		**nqi**		
blocked R160Q hSO	^{33}S	2.1	(1.6, 2.5, −4.1)	36	0.2	this work
	$^{17}O_{coordinated}$	−9	(5, 5, −10)	7	–	
	$^{17}O_{remote}$	−4.5	(1.25, 1.25, −2.5)	5	–	
blocked wt hSO*†	^{33}S	2.6	(−0.3, −0.3, 0.6)	36	–	27
blocked At-SO*	^{33}S	3.3	(1.3, 1.5, −2.8)	40	0	23
SO-Sulfate (DFT)	^{33}S	3.33	(−0.53, −0.40, 0.92)	4.4	0.7	this work
	$^{17}O_{coordinated}$	−9.56	(6.06, 5.17, −11.22)	10.9	0.3	
	$^{17}O_{remote}$	−1.23 (a)	(1.18, 1.17, −2.35)	10.6	0.1	
		0.02 (b)	(0.00, −0.36, 0.36)	10.5	0.1	
		0.01 (c)	(0.00, −0.27, 0.27)	10.9	0.1	
	$^{17}O_{oxo}$	3.26	(−3.71, −2.34, 6.04)	1.2	1.0	
SO-Sulfite (DFT)	^{33}S	1.91	(−0.69, −0.45, 1.14)	27.9	0.2	this work
	$^{17}O_{coordinated}$	−11.09	(9.34, 8.41, −17.75)	9.6	0.4	
	$^{17}O_{remote}$	−1.71 (a)	(1.66, 1.60, −3.26)	9.5	0.3	
		−0.10 (b)	(0.08, 0.45, −0.53)	9.9	0.1	
	$^{17}O_{oxo}$	3.61	(−4.38, −0.24, 4.62)	1.1	1.0	

*The ^{17}O magnetic resonance parameters for these species have not been fully evaluated. †The *blocked* form of this enzyme was obtained only under low-pH conditions in the strict absence of Cl⁻.

the entire EPR spectrum by ED-NMR. In two-pulse ESEEM, the coordinated ^{17}O signal dominated g_y and g_x and showed well-resolved *nqi* related splittings only at g_x. Unfortunately, we were unable to observe the spectrum of the coordinated ^{17}O at the g_z position at either K_a- or W-band, which impeded the complete experimental interpretation of the spectra. However, this lack of information was partially circumvented by simulations and the DFT calculations discussed below.

3. DFT Estimates of the SO Magnetic Resonance Parameters. In addition to the efforts described above to chemically distinguish between coordinated sulfate and sulfite as the Mo(V)-bound ligand of species 1, the magnetic resonance parameters for each possibility were also calculated using DFT methods, as described in the Materials and Methods section. As we (and others) have previously demonstrated,[11,18,29,30,65] the structure of an unknown system can be inferred through the general agreement or disagreement of its spectroscopic parameters with those calculated from theory for a given model. The goal of the calculations is not to exactly replicate the experimental results by calculating the properties for a very large number of conceivable models. Rather, the calculated magnetic resonance parameters serve to distinguish unique structural possibilities from one another by evaluating the overall fit of their calculated results to each other and to the experimental results, as in the case of sulfate versus sulfite coordination to Mo(V).

Recently, we reported our initial attempt to investigate the broad differences in the magnetic resonance parameters of sulfate- and sulfite-bound Mo(V) SO using DFT.[11] In that work, two minimal structural models (about 30 atoms each) having ^{17}O- and ^{33}S-labeled oxo-Mo(V)-sulfate/sulfite centers were prepared on the basis of the crystal structure of chicken SO, and the relevant parameters were then calculated. The results from these models provided the first indication that the weakly coupled ^{17}O observed experimentally could possibly originate from a remote oxygen of either coordinated sulfate or sulfite instead of from the axial oxo ligand. Furthermore, significant differences in the ^{33}S magnetic resonance parameters existed between the two models that seemed to favor the sulfite model, particularly in their *nqi* values. The *hfi* constants for the ^{33}S and coordinated ^{17}O of the sulfate and sulfite ligands, however, provided no conclusive information about the identity of the ligand, since the *hfi* is highly sensitive to the specific orientation of the bound ligands, which would normally be constrained by the steric and H-bonding interactions within the substrate-binding pocket of the enzyme (see Figure 1).[6] Furthermore, the validity of the *nqi* results, however similar their agreement may be to the experimental values, must be questioned in such minimal systems that do not adequately model the electric field gradient surrounding the atoms of interest, since protein and exogenous water interactions were not included. For these reasons, more complete models were prepared that include the entire binding pocket and allow the orientation of the sulfate and sulfite ligands to be more realistically represented.

Figure 9 shows the geometry-optimized structural representations of the sulfate- and (one of the) sulfite-coordinated DFT models. Each of these contains about 250 atoms (the *xyz* coordinates for each model are provided in the Supporting Information). Although the rotation of sulfate is effectively constrained by its high symmetry (tetrahedral), sulfite could arguably exist in at least three principal orientations, since it is trigonal pyramidal. The effects of these orientations were investigated by running separate sets of calculations for three

orientations of sulfite. The results for only one of the sulfite models will be discussed here, since the calculated parameters of all of the models were effectively identical. The relevant calculated magnetic resonance parameters for the sulfate model and one of the sulfite models are included in Table 1 for comparison to each other and to the corresponding experimental results. The parameters for these and the additional sulfite models are included in Table S1. Due to the extreme hardware and time demands required to complete such work (thousands of processor-core-hours), *wt* SO, having an Arg residue instead of Gln (as in species 1, for example) *trans* to the axial oxo ligand of the Mo center, was chosen for the first large DFT model. Therefore, the results of these models could arguably be more relevant to the *blocked* form of *wt* At-SO. The experimentally determined magnetic resonance parameters for all *blocked* forms are similar,[23,24,31] however, justifying any comparison of the calculated parameters to *blocked* forms in general. The effects of specific active site mutations on the magnetic resonance parameters of *blocked* SO will be addressed in future work.

To our knowledge, no synthetic sulfate or sulfite model compounds that even remotely represent the proposed active site structure of *blocked* SOEs in the Mo(V) state have been reported to date. This is most likely due to the very poor binding properties of either ligand. Within a protein environment, however, positively charged amino acid side chains are able to greatly stabilize the binding of these otherwise weak ligands. Indeed, our DFT models demonstrate that both sulfate and sulfite form stable bonds to the Mo(V) of SO within the protein, and each ligand is further stabilized by multiple H-bonding interactions from nearby residues. The optimized Mo(V)−O$_{sulfate}$ bond (2.17 Å) was determined to be slightly weaker than that of Mo(V)−O$_{sulfite}$ (2.11 Å), but both bond lengths compared well to values we have determined in our previous calculations for Mo(V)−OH centers (2.05−2.2 Å).[18,30]

In contrast, there are measurable differences between the calculated magnetic resonance parameters of sulfate and sulfite. The magnitude of the ^{33}S nuclear quadrupole coupling constants (χ), most notably, differs by a factor of ~7. For sulfate, in which the sulfur is located within a very symmetric electric field, a value of ~4.4 MHz is obtained, while a value of ~28 MHz is obtained for sulfite. Comparison of the calculated and experimentally measured χ values for ^{33}S strongly favors the sulfite model (Table 1). No other significant differences exist between the magnetic resonance parameters of sulfate and sulfite.

As previously mentioned, the orientation of the exchangeable equatorial ligand has a large effect on the spin population delocalization from the Mo(V) d_{xy} orbital onto the exchangeable ligand. This is clearly observed in the values of the remote ^{17}O *hfi* constants, where one of the nuclei has a large *hfi* while the others are small despite their chemical equivalency. The calculated *hfi* constants of the sulfate and sulfite remote ^{17}O nuclei compare well to the experimentally determined values, although both are underestimated. Interestingly, the *nqi* of these nuclei (9.5−10.9 MHz) are much larger than those of the ^{17}O oxo, which are around 1−1.5 MHz, as determined by both experiment and calculation.[29] The large difference between the oxo and remote oxygen *nqi* (~10 fold) lends further support to our (re)assignment of the exchangeable ^{17}O of the *blocked* forms (*nqi* ~5 MHz) to remote oxygens rather than to an "oxo" group. Despite improvements in the DFT models, the calculated *nqi* values (Table 1) still differ from experiment by a factor of 2, which could possibly be explained by an under-representation of the H-bonding of the
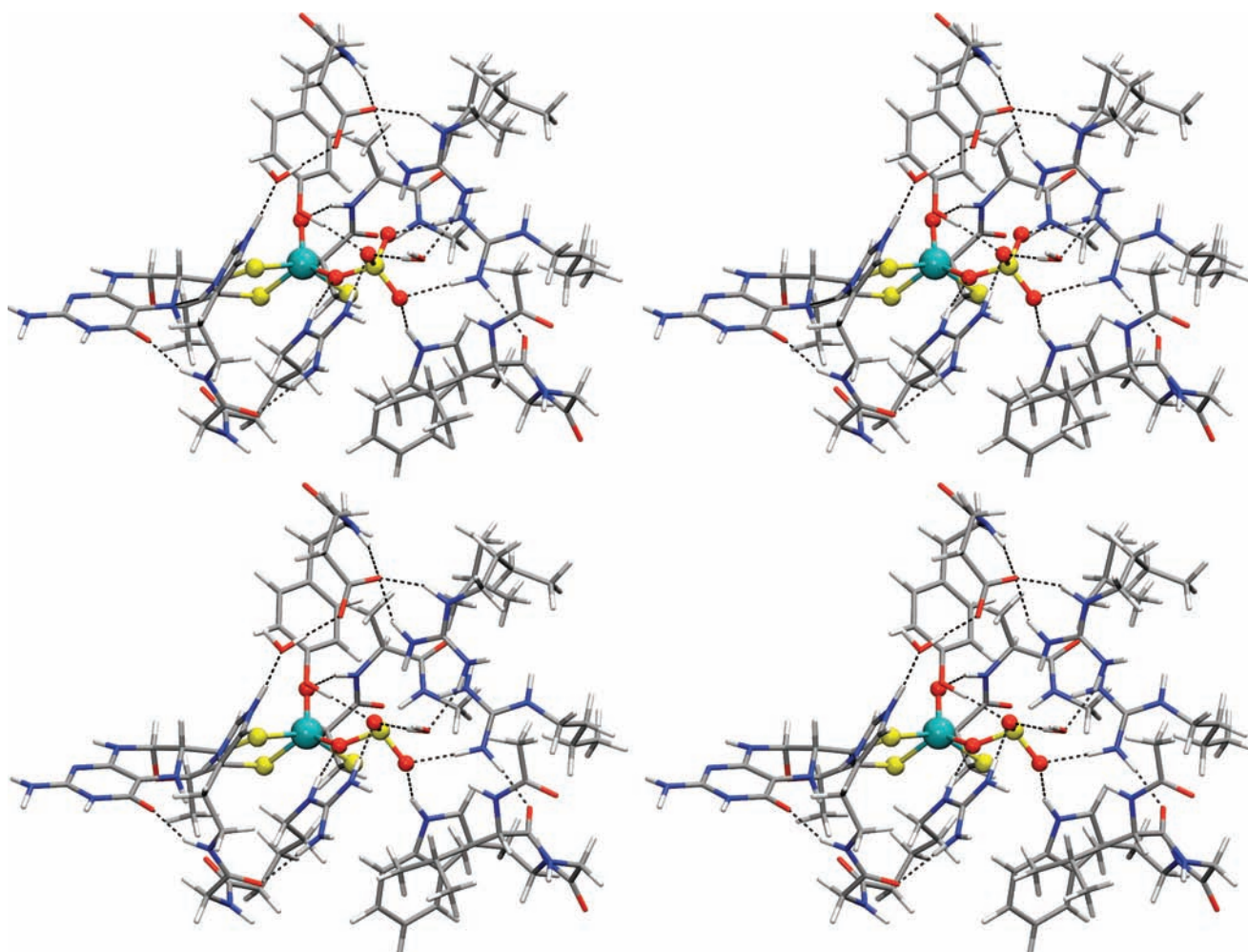
Figure 9. Stereoview (cross-eye) representations of the energy-minimized sulfate- and sulfite-bound SO models (upper and lower, respectively). The magnetic resonance parameters calculated for these models are provided in Table 1, and the atom coordinates are provided in the Supporting Information. blue-green = Mo, red = O, yellow = S, gray = C, and blue = N.

amino acid side chains and/or exogenous water molecules with sulfite. This effect was recently demonstrated from DFT calculations for [17]O water bound to Gd(III), where the [17]O χ could be decreased from 10 to 6.1 MHz depending only on H-bonding interactions.[66] Regardless, on the basis of these DFT results and our experimental work involving phosphate and CaCl$_2$, it is clear that the axial oxo group of the Mo(V) center of species 1 of R160Q hSO does not exchange with [17]O. Thus, there is no need to invoke the previously proposed axial interaction of Gln with the Mo(V) center of R160Q to explain the unusual [17]O *nqi* value. Rather, the apparent increase in the "oxo" *nqi* of the *blocked* forms should be attributed to the remote oxygen atoms of the exchangeable sulfite ligand, which is known to rapidly and spontaneously exchange its oxygens with water.[33]

■ **CONCLUSION**

At low pH the fatal R160Q mutant of hSO produces species 1, which was previously ascribed to a six-coordinate Mo(V) center with an exchangeable terminal oxo ligand and an equatorial sulfate group.[23,28,31] In this work, pulsed EPR experiments and DFT calculations provide compelling evidence that the exchangeable ligand of species 1 is sulfite (Figure 1 and Scheme 1). Thus, the original proposal by Bray regarding the existence of a "sulfite" form of SO is correct, in principle.[67]

The transformation of species 1 into the phosphate-inhibited form clearly demonstrates that the weakly coupled [17]O, observed in ESEEM experiments, belongs to sulfite and not to the axial oxo. Furthermore, the need to invoke a ligand interaction with Mo(V) *trans* to the oxo,[28] thereby increasing the axial [17]O-oxo *nqi*,[31] is unnecessary.

Finally, this comprehensive study of the *blocked* form (species 1) of R160Q by isotopic labeling, variable frequency pulsed EPR spectroscopy, and large-scale DFT calculations demonstrates the utility of these combined procedures for elucidating the roles of anions, mutations, and steric factors in the formation, stabilization, and transformation of active site complexes of SOEs that may be involved in catalysis and/or inhibition. This integrated approach should also be applicable to direct interrogation of the paramagnetic states in the catalytic cycles of other metalloproteins.

■ **ASSOCIATED CONTENT**

ⓈSupporting Information

Specific details regarding the generation of the *Pi* and standard *lpH* forms of R160Q hSO from (*blocked*) species 1, a full description of the EPR simulation procedures, the optimized atom coordinates of the sulfate- and sulfite-bound enzyme models from which all of the DFT-calculated magnetic resonance parameters were derived, figures depicting the

calculated *g*-tensor orientations and total spin density contours of each model, Euler rotations of the electric field gradient (EFG) and hyperfine tensors of relevant atoms to the *g*-tensor, magnetic field positions corresponding to specific ESEEM measurements, and a summary table of all of the experimental and calculated magnetic resonance parameters relevant to this work. This material is available free of charge via the Internet at http://pubs.acs.org.

■ AUTHOR INFORMATION

Corresponding Author

*E-mail: daniella.goldfarb@weizmann.ac.il; jenemark@email.arizona.edu.

■ ACKNOWLEDGMENTS

■ REFERENCES

(1) Hille, R. *Chem. Rev.* **1996**, *96*, 2757−2816.
(2) Feng, C.; Tollin, G.; Enemark, J. H. *Biochim. Biophys. Acta* **2007**, *1774*, 527−539.
(3) Johnson, J. L. *Prenatal Diagn.* **2003**, *23*, 6−8.
(4) Tan, W. H.; Eichler, F. S.; Hoda, S.; Lee, M. S.; Baris, H.; Hanley, C. A.; Grant, E.; Krishnamoorthy, K. S.; Shih, V. E. *Pediatrics* **2005**, *116*, 757−766.
(5) Dublin, A. B.; Hald, J. K.; Wootton-Gorges, S. L. *Am. J. Neuroradiol.* **2002**, *23*, 484−485.
(6) Kisker, C.; Schindelin, H.; Pacheco, A.; Wehbi, W. A.; Garrett, R. M.; Rajagopalan, K. V.; Enemark, J. H.; Rees, D. C. *Cell* **1997**, *91*, 973−983.
(7) Schrader, N.; Fischer, K.; Theis, K.; Mendel, R. R.; Schwarz, G.; Kisker, C. *Structure* **2003**, *11*, 1251−1263.
(8) George, G. N.; Kipke, C. A.; Prince, R. C.; Sunde, R. A.; Enemark, J. H.; Cramer, S. P. *Biochemistry* **1989**, *28*, 5075−5080.
(9) Karakas, E.; Wilson, H. L.; Graf, T. N.; Xiang, S.; Jaramillo-Busquets, S.; Rajagopalan, K. V.; Kisker, C. *J. Biol. Chem.* **2005**, *280*, 33506−33515.
(10) Kappler, U.; Bailey, S. *J. Biol. Chem.* **2005**, *280*, 24999−25007.
(11) Enemark, J. H.; Raitsimring, A. M.; Astashkin, A. V.; Klein, E. L. *Faraday Discuss.* **2011**, *148*, 249−267.
(12) Pacheco, A.; Basu, P.; Borbat, P.; Raitsimring, A. M.; Enemark, J. H. *Inorg. Chem.* **1996**, *35*, 7001−7008.
(13) Bray, R. C. *Q. Rev. Biophys.* **1988**, *21*, 299−329.
(14) Gutteridge, S.; Lamy, M. T.; Bray, R. C. *Biochem. J.* **1980**, *191*, 285−288.
(15) Lamy, M. T.; Gutteridge, S.; Bray, R. C. *Biochem. J.* **1980**, *185*, 397−403.
(16) Bray, R. C.; Gutteridge, S.; Lamy, M. T.; Wilkinson, T. *Biochem. J.* **1983**, *211*, 227−236.
(17) Doonan, C. J.; Wilson, H. L.; Bennett, B.; Prince, R. C.; Rajagopalan, K. V.; George, G. N. *Inorg. Chem.* **2008**, *47*, 2033−2038.
(18) Klein, E. L.; Astashkin, A. V.; Ganyushin, D.; Riplinger, C.; Johnson-Winters, K.; Neese, F.; Enemark, J. H. *Inorg. Chem.* **2009**, *48*, 4743−4752.
(19) Enemark, J. H.; Astashkin, A. V.; Raitsimring, A. M. High-Resolution EPR Spectroscopy of Mo Enzymes. Sulfite Oxidases: Structural and Functional Implications. In *Biological Magnetic Resonance*; Hanson, G., Berliner, L. J., Eds.; Springer: 2010; Vol. 29, pp 122−162.
(20) Enemark, J. H.; Astashkin, A. V.; Raitsimring, A. M. *Dalton Trans.* **2006**, 3501−3514.
(21) Bray, R. C. In *Biological Magnetic Resonance*; Berliner, L. J., Reuben, J., Eds.; Plenum Press: New York, 1980; Vol. 2, p 45.
(22) At-SO contains no integral electron acceptor (e.g., heme). For this reason, an external oxidant is required to produce the Mo(V) intermediate of the enzyme from its fully reduced form.
(23) Astashkin, A. V.; Johnson-Winters, K.; Klein, E. L.; Byrne, R. S.; Hille, R.; Raitsimring, A. M.; Enemark, J. H. *J. Am. Chem. Soc.* **2007**, *129*, 14800−14810.
(24) Astashkin, A. V.; Hood, B. L.; Feng, C. J.; Hille, R.; Mendel, R. R.; Raitsimring, A. M.; Enemark, J. H. *Biochemistry* **2005**, *44*, 13274−13281.
(25) Rapson, T. D.; Astashkin, A. V.; Johnson-Winters, K.; Bernhardt, P. V.; Kappler, U.; Raitsimring, A. M.; Enemark, J. H. *J. Biol. Inorg. Chem.* **2010**, *15*, 505−514.
(26) Raitsimring, A. M.; Astashkin, A. V.; Feng, C.; Wilson, H. L.; Rajagopalan, K. V.; Enemark, J. H. *Inorg. Chim. Acta* **2008**, *361*, 941−946.
(27) Rajapakshe, A.; Johnson-Winters, K.; Nordstrom, A. R.; Meyers, K. T.; Emesh, S.; Astashkin, A. V.; Enemark, J. H. *Biochemistry* **2010**, *49*, 5154−5159.
(28) Doonan, C. J.; Wilson, H. L.; Rajagopalan, K. V.; Garrett, R. M.; Bennett, B.; Prince, R. C.; George, G. N. *J. Am. Chem. Soc.* **2007**, *129*, 9421−9428.
(29) Astashkin, A. V.; Neese, F.; Raitsimring, A. M.; Cooney, J. J. A.; Bultman, E.; Enemark, J. H. *J. Am. Chem. Soc.* **2005**, *127*, 16713−16722.
(30) Astashkin, A. V.; Klein, E. L.; Ganyushin, D.; Johnson-Winters, K.; Neese, F.; Kappler, U.; Enemark, J. H. *Phys. Chem. Chem. Phys.* **2009**, *11*, 6733−6742.
(31) Astashkin, A. V.; Johnson-Winters, K.; Klein, E. L.; Feng, C. J.; Wilson, H. L.; Rajagopalan, K. V.; Raitsimring, A. K.; Enemark, J. H. *J. Am. Chem. Soc.* **2008**, *130*, 8471−8480.
(32) Astashkin, A. V.; Feng, C.; Raitsimring, A. M.; Enemark, J. H. *J. Am. Chem. Soc.* **2005**, *127*, 502−503.
(33) Betts, R. H.; Voss, R. H. *Can. J. Chem.* **1970**, *48*, 2035−2041.
(34) Astashkin, A. V.; Enemark, J. H.; Raitsimring, A. M. *Concepts Magn. Reson., Part B (Magn. Reson. Eng.)* **2006**, *29B*, 125−136.
(35) Goldfarb, D.; Lipkin, Y.; Potapov, A.; Gorodetsky, Y.; Epel, B.; Raitsimring, A. M.; Radoul, M.; Kaminker, I. *J. Magn. Reson.* **2008**, *194*, 8−15.
(36) Höfer, P.; Grupp, A.; Nebenführ, H.; Mehring, M. *Chem. Phys. Lett.* **1986**, *132*, 279−282.
(37) http://quiz2.chem.arizona.edu/epr.
(38) http://www.thch.uni-bonn.de/tc/orca.
(39) Becke, A. D. *Phys. Rev. A* **1988**, *38*, 3098−3100.
(40) Perdew, J. P. *Phys. Rev. B* **1986**, *33*, 8822−8824.
(41) Becke, A. D. *J. Chem. Phys.* **1993**, *98*, 5648−5652.
(42) Lee, C.; Yang, W.; Parr, R. P. *Phys. Rev. B* **1988**, *37*, 785−789.
(43) Schäfer, A.; Huber, C.; Ahlrichs, R. *J. Chem. Phys.* **1994**, *100*, 5829−5835.
(44) Schäfer, A.; Horn, H.; Ahlrichs, R. *J. Chem. Phys.* **1992**, *97*, 2571−2577.
(45) Weigend, F.; Haeser, M.; Patzelt, H.; Ahlrichs, R. ftp://ftp.chemie-karlsruhe.de/pub/basen.
(46) van Lenthe, E.; Baerends, E. J.; Snijders, J. G. *J. Chem. Phys.* **1993**, *99*, 4597−4610.
(47) van Wüllen, C. *J. Chem. Phys.* **1998**, *109*, 392−399.
(48) van Lenthe, J. H.; Faas, S.; Snijders, J. G. *Chem. Phys. Lett.* **2000**, *328*, 107−112.

1417

dx.doi.org/10.1021/ic201643t | *Inorg. Chem.* 2012, 51, 1408−1418

(49) Klamt, A.; Schüürmann, G. *J. Chem. Soc., Perkin Trans. 2* **1993**, 799−805.

(50) Sinnecker, S.; Neese, F. *J. Comput. Chem.* **2006**, *27*, 1463−1475.

(51) Roy, A. *Isr. J. Chem.* **1967**, *5*, 4.

(52) Nilsson, G.; Rengemo, T.; Sillen, L. G. *Acta Chem. Scand.* **1958**, *12*, 868−872.

(53) While carrying out the experiments described in ref 27 for various forms of SO, attempts were made to convert species 1 into the *lpH* form by adding sodium chloride. No effect of the chloride addition was detectable, even at concentrations of 1 M NaCl.

(54) *Reagent Chemicals: Specifications and Procedures: American Chemical Society Specifications*; American Chemical Society: 2006.

(55) Dikanov, S. A.; Liboiron, B. D.; Thompson, K. H.; Vera, E.; Yuen, V. G.; McNeill, J. H.; Orvig, C. *J. Am. Chem. Soc.* **1999**, *121*, 11004−11005.

(56) Schosseler, P.; Wacker, T.; Schweiger, A. *Chem. Phys. Lett.* **1994**, *224*, 319−324.

(57) Kulik, L.; Epel, B.; Messinger, J.; Lubitz, W. *Photosynth. Res.* **2005**, *84*, 347−353.

(58) Jeschke, G.; Spiess, H. W. *Chem. Phys. Lett.* **1998**, *293*, 9−18.

(59) Potapov, A.; Epel, B.; Goldfarb, D. *J. Chem. Phys.* **2008**, *128*, 052320-1−052320-10.

(60) Kaminker, I.; Goldberg, H.; Neumann, R.; Goldfarb, D. *Chem.—Eur. J.* **2010**, *16*, 10014−10020.

(61) Florent, M.; Kaminker, I.; Nagarajan, V.; Goldfarb, D. *J. Magn. Reson.* **2011**, *210*, 192−199.

(62) Astashkin, A. V.; Dikanov, S. A.; Kurshev, V. V.; Tsvetkov, Y. D. *Chem. Phys. Lett.* **1987**, *136*, 335−341.

(63) The maximum π-pulse amplitude achievable with the W-band instrumentation used in these measurements does not exceed 20 MHz,[35] while B_1 = ~40 MHz was used in the Ka-band measurements.

(64) Raitsimring, A. M.; Astashkin, A. V.; Baute, D.; Goldfarb, D.; Caravan, P. *J. Phys. Chem. A* **2004**, *108*, 7318−7323.

(65) Neese, F. *Coord. Chem. Rev.* **2009**, *253*, 526−563.

(66) Yazyev, O. V.; Helm, L. *J. Chem. Phys.* **2006**, *125*, 0545031−0545038.

(67) Bray, R. C.; Lamy, M. T.; Gutteridge, S.; Wilkinson, T. *Biochem. J.* **1982**, *201*, 241−243.

(68) van Doorslaer, S.; Schweiger, A. *Chem. Phys. Lett.* **1997**, *281*, 297−305.

(69) Astashkin, A. V.; Raitsimring, A. M. *J. Magn. Reson.* **2000**, *143*, 280−291.